Numerical simulation of early-age shrinkage effects on RC member deflections and cracking development

P. Bernardi, R. Cerioni, E. Michelini, A. Sirico
Dept. of Civil, Environmental, Land Management Engineering and Architecture, University of Parma (Italy)
patrizia.bernardi@unipr.it, roberto.cerioni@unipr.it, elena.michelini@unipr.it, alice.sirico@studenti.unipr.it

ABSTRACT. Shrinkage effects on short-term behavior of reinforced concrete elements are often neglected both in design code provisions and in numerical simulations. However, it is known that their influence on serviceability performance can be significant, especially in case of lightly-reinforced beams. As a matter of fact, the restraint provided by the reinforcement on concrete determines a reduction of the cracking load of the structural element, as well as an increase of its deflection. This paper deals with the modeling of early-age shrinkage effects in the field of smeared crack approaches. To this aim, an existing non-linear constitutive relation for cracked reinforced concrete elements is extended herein to include early-age concrete shrinkage. Careful verifications of the model are carried out by comparing numerical results with significant experimental data reported in technical literature, providing a good agreement both in terms of global and local behavior.

KEYWORDS. Reinforced concrete; Shrinkage; Cracking; Short-term loading; Non-linear analysis; FEM.

INTRODUCTION

In the design of reinforced concrete (RC) members, creep and shrinkage effects are usually taken into account for the evaluation of long-term deflections and pre-stress losses. It is indeed well known that these phenomena have a significant influence on the behavior of RC elements under sustained loads, by increasing their deformations and crack width over time. On the contrary, their effects on short-term response are often disregarded [1, 2]. Several theoretical and experimental works (among others, e.g. [3, 4]) have however pointed out that the restraining of concrete shrinkage (usually due to the presence of embedded reinforcement) significantly affects the cracking resistance of structural elements, as well as their deformations even under short-term loading. As a consequence, a proper numerical modelling should consider this effect, so as to avoid inaccurate predictions of structural performances at serviceability conditions. To this aim, concrete shrinkage can be explicitly considered by treating it as a prescribed deformation or as a fictitious force in the analyses [5-9].
In this work, an existing smeared-crack model for RC elements subjected to in-plane stresses, named 2D-PARC [10-12], is extended so as to correctly take into account early-age shrinkage effects. In more detail, concrete shrinkage is rigorously modelled by inserting it explicitly into 2D-PARC general algorithm as a prescribed deformation. The effectiveness of the proposed procedure is verified herein through the modelling of two experimental programs [13, 14] on RC shrunk beams with low reinforcement ratio tested to short-term bending. These elements are highly sensitive to shrinkage effects, especially in presence of a non-symmetric arrangement of steel reinforcement in the element cross-section. The restraint

provided by embedded bars produces indeed a not uniform distribution of induced tensile stresses in concrete, with a consequent initial warping of the member. Comparisons between numerical and experimental results prove that the proposed approach is able to correctly catch the effects of concrete shrinkage strains on member deflection, as well as on cracking strength and development.

NUMERICAL MODEL

In this work, the original formulation of 2D-PARC constitutive relation is properly revised so as to include concrete shrinkage effects in short-term analyses. As already mentioned, this model, which is based on a smeared-fixed crack approach, was developed for a concrete membrane element containing *n* reinforcing layers with different orientations, subjected to plane stress conditions. The main features of 2D-PARC, as well as its governing equations can be found in [10-12], to which reference is made. In the following Sections the attention will be only focused on the main changes made to the original structure of the model in order to include concrete shrinkage.

Uncracked stage

In the uncracked stage, perfect bond is assumed between steel bars and the surrounding concrete, so the total strain vector $\{\varepsilon\}$ is coincident with the strain in concrete $\{\varepsilon_c\}$ and steel $\{\varepsilon_s\}$:

$$\{\varepsilon\} = \{\varepsilon_c\} = \{\varepsilon_s\}, \tag{1}$$

The total stress vector $\{\sigma\}$ can be then simply evaluated as the sum of the stresses acting in concrete, $\{\sigma_c\}$, and in steel reinforcement, $\{\sigma_s\}$. To take into account shrinkage effects, concrete stresses $\{\sigma_c\}$ are here computed as a function of concrete net strains ($\{\varepsilon_c\}$ - $\{\varepsilon_{sh}\}$), being $\{\varepsilon_{sh}\}$ the free shrinkage strain vector. According to 2D-PARC conventions, free shrinkage strains are assumed as negative, since they cause concrete shortening. The terms of vector $\{\varepsilon_{sh}\}$ can be either set equal to the shrinkage strain values measured during experimental tests, if available, or properly calculated according to classical formulations obtained from technical literature (e.g. [15-17]). In any case, the component of $\{\varepsilon_{sh}\}$ associated to shear strains is usually assumed equal to zero. The equilibrium equation for the uncracked RC element can be then written as:

$$\{\sigma\} = \{\sigma_c\} + \{\sigma_s\} = [D_c] \left(\{\varepsilon_c\} - \{\varepsilon_{sh}\} \right) + [D_s] \{\varepsilon_s\}, \tag{2}$$

where $[D_c]$ and $[D_s]$ respectively represent concrete and steel stiffness matrix, whose construction has been discussed elsewhere ([10] and [12], in a more recently revised form).

Cracked stage

Crack formation takes place when the current state of stress violates the concrete failure envelope in the cracking region (see [12]). In presence of shrinkage, the transition from uncracked to cracked stage occurs in correspondence of a lower load level, since the restraint provided by the embedded reinforcement causes the appearance of tensile stresses in concrete even before the application of any external load. Crack pattern is hypothesized to develop with a constant spacing a_{m1} and a strain decomposition procedure is adopted, so leading to the following compatibility condition:

$$\{\varepsilon\} = \{\varepsilon_c\} + \{\varepsilon_{cr1}\}, \tag{3}$$

where the total strain vector $\{\varepsilon\}$ is obtained as the sum of the strains $\{\varepsilon_c\}$ in RC between two adjacent cracks (still intact, even if damaged), and those in the fracture zone, $\{\varepsilon_{cr1}\}$, related to all the kinematics that develop after crack formation. As known, crack opening and sliding activate indeed several resistant mechanisms, such as aggregate bridging and interlock, tension stiffening and dowel action, which provide strength and stiffness. According to the procedure described in [10], the two strain vectors, $\{\varepsilon_c\}$ and $\{\varepsilon_{cr1}\}$, are obtained by inverting the equilibrium conditions in the uncracked RC between cracks and at crack location, respectively. Moreover, the stresses in RC between adjacent cracks, $\{\sigma_c\}$, and those in the crack, $\{\sigma_{cr1}\}$, are assumed to be coincident with each other and consequently to the total stress vector $\{\sigma\}$.
In more detail, the equilibrium condition in RC between cracks is formally identical to Eq. 2, even if concrete and steel stiffness matrices, $[D_c]$ and $[D_s]$, are slightly modified with respect to the uncracked stage, so as to consider the degradation

that occurs after cracking, as explained in [10, 12]. Moreover, since in the cracked stage the hypothesis of perfect bond is no longer valid (and consequently the two strain vectors $\{\varepsilon_c\}$ and $\{\varepsilon_s\}$ cannot be set equal to each other), the steel strain $\{\varepsilon_s\}$ is assumed coincident with the total average strain $\{\varepsilon\}$, with a negligible approximation in excess. By inverting the equilibrium condition in RC between cracks, concrete strains $\{\varepsilon_c\}$ can be then expressed as:

$$\{\varepsilon_c\} = [D_c]^{-1}\left(\{\sigma\} - [D_s]\{\varepsilon\}\right) + \{\varepsilon_{sh}\}. \tag{4}$$

The strain vector $\{\varepsilon_{cr1}\}$ can be in turn determined by inverting the equilibrium equation at crack location:

$$\{\varepsilon_{cr1}\} = [D_{cr1}]^{-1}\{\sigma\}, \tag{5}$$

being $[D_{cr1}]$ the crack stiffness matrix, whose expression – which is not modified in presence of shrinkage – can be still found in [10].
By substituting Eqs 4 and 5 into the compatibility Eq. 3, the total stress $\{\sigma\}$ vector in case of shrinkage can be then expressed as follows:

$$\{\sigma\} = \left([D_c]^{-1} + [D_{cr1}]^{-1}\right)^{-1}\left\{\left([I] + [D_c]^{-1}[D_s]\right)\{\varepsilon\} - \{\varepsilon_{sh}\}\right\}, \tag{6}$$

being $[I]$ the identity matrix.

MODEL VALIDATION

The effectiveness of the above described procedure, as well as of its correct implementation into a commercial finite element (FE) code (ABAQUS), are verified herein through comparisons with detailed test data on shrunk RC beams subjected to short-term bending. The first considered experimental program (carried out by Gribniak, [13]) mainly focuses on the effects of concrete shrinkage on beam deflection and first cracking moment in case of different amounts of top reinforcement, while the second one (by Sato et al. [14]) compares the flexural behavior of RC beams subjected or not to shrinkage prior to loading.

Numerical vs. experimental results for RC beams with different amounts of top reinforcement [13]

Four RC beams tested by Gribniak [13] – respectively named S1, S1R, S2, S2R – and subjected to four-point bending are first analyzed. The considered specimens were characterized by the same geometry, with a rectangular cross-section (300 mm deep and 280 mm wide) and a total length equal to 3280 mm, with a net span of 3000 mm. Series 1 and 2 were obtained from different concrete batches, showing slightly different compressive strengths f_c, as reported in Tab. 1.

Sample	Steel				Concrete		
	$A_{s,bottom}$ [mm²]	$A_{s,top}$ [mm²]	E_s [GPa]	f_{sy} [MPa]	f_c [MPa]	ε_{sh} (10^{-6})	φ_c
S1	309.0	56.6	212	566	47.3	-194.6	1.6
S1R	309.0	749	212	566	47.3	-188.2	1.6
S2	309.0	56.6	212	566	48.7	-152.6	1.4
S2R	309.0	749	212	566	48.2	-155.7	1.4

Table 1: Material properties of RC beams tested by Gribniak [13].

All the specimens contained the same amount of lower tensile reinforcement (denoted as $A_{s,bottom}$ in Tab. 1, corresponding to 4ϕ10 mm bars), as well as of transverse reinforcement (ϕ6 mm / 100 mm spaced). The two specimens with designation "R" had an higher amount of top reinforcement ($A_{s,top}$, Tab. 1), constituted by 3ϕ18 mm bars, instead of 2ϕ6 mm bars. The main mechanical properties of steel reinforcement are summarized in Tab. 1 for reading convenience, together with

concrete compressive strength f_c, shrinkage strains ε_{sh} and creep coefficient φ_c measured at the test date (see [13] for details). The experimental value of ε_{sh} is used herein to compose the shrinkage strain vector that must be defined in the numerical model, as described in the previous Section. Since shrinkage-induced stresses develop gradually with time, the relief caused by creep should be included in numerical simulations, as suggested by many Authors in the literature (e.g., [1, 8]). The creep coefficient φ_c reported in Tab. 1 is therefore adopted in the initial step of the analyses to correct the stresses in concrete, by applying the effective modulus method [1].

All tests were carried out under loading control. On the contrary, numerical analyses are performed under displacement control, in order to achieve a better numerical convergence. Taking advantage of the symmetry of the problem, only one half of each beam is simulated, by adopting a FE mesh constituted by quadratic, isoparametric 8-node membrane elements with reduced integration (4 Gauss integration points).

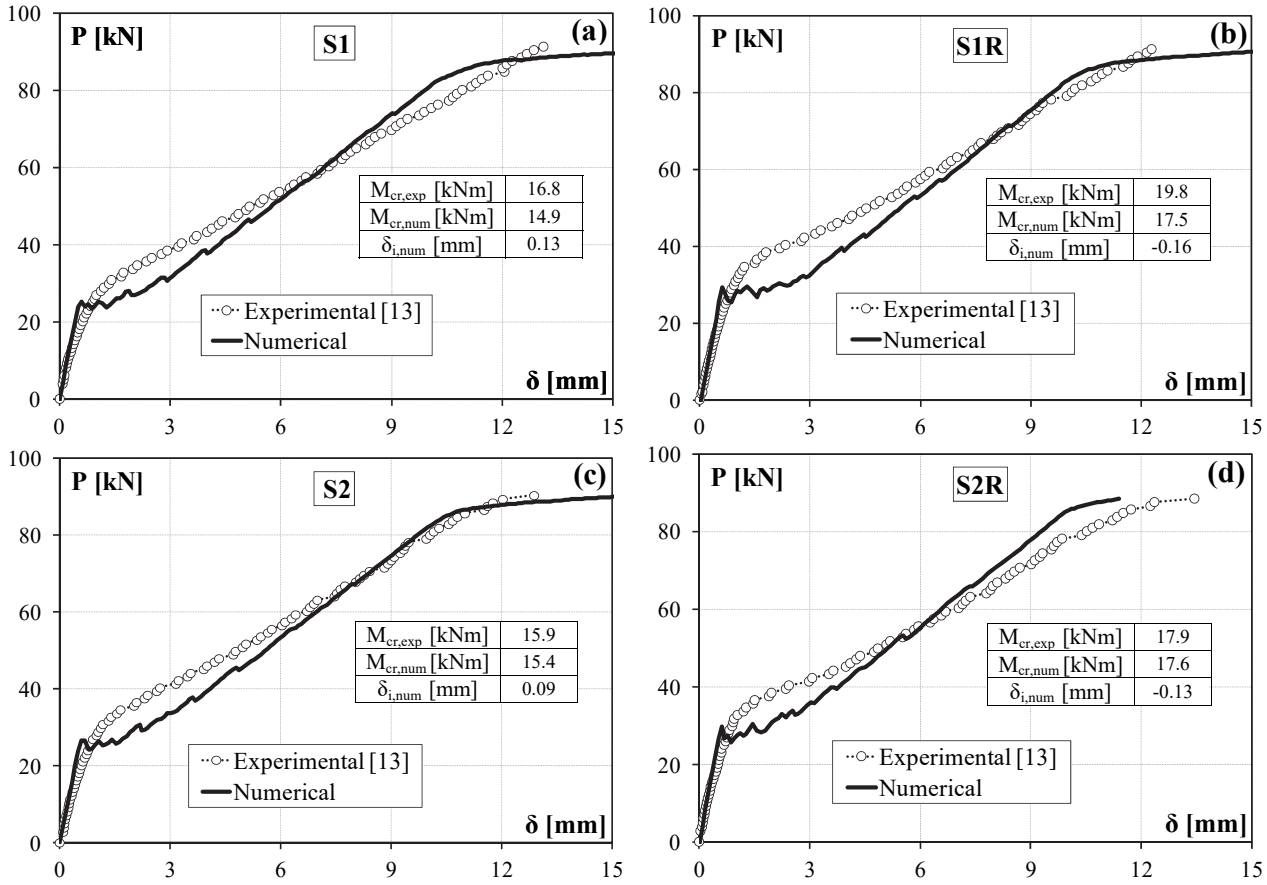

Figure 1: Comparison between numerical and experimental [13] results in terms of total applied load P vs. midspan deflection δ for beams: (a) S1; (b) S1R; (c) S2; (d) S2R.

A first comparison between numerical and experimental results is provided in Fig. 1, in terms of total applied load P vs. midspan deflection δ. Since the initial deflection due to shrinkage was not experimentally measured, numerical analyses are shifted to the origin along the horizontal axis, so as to match experimental results. The values of initial shrinkage deflection δ_i, as obtained from numerical analyses before the application of external loading, is however reported in each graph of Fig. 1.

A good agreement is found for all the considered specimens. Beams with a larger amount of top reinforcement (designation "R", Fig. 1b,d) are characterized by an initial negative deflection δ_i due to shrinkage. Moreover, they show an higher cracking resistance with respect to their twin specimens (Fig. 1a,c). This can be attributable to the increment of moment of inertia due to the presence of a heavier top reinforcement, but mainly to the difference of tensile stresses caused by shrinkage in the extreme bottom fiber of the cross-section. To better clarify this last aspect, the numerical variation within the depth of the section of the total strain ε, as well as of the stresses in concrete σ_c and in steel σ_s just before loading are reported in Fig. 2 for the twin beams S1 and S1R. The presence of a not symmetric reinforcement in the beam cross-section determines a not uniform restraint to free shrinkage, which in turn causes the element curvature

and the appearance of a stress gradient. Heavy compressive reinforcement (S1R specimen) provides a larger restraint to the top of the beam, so leading to a reversed curvature and to a great reduction of tensile shrinkage stresses in the extreme bottom fiber. For this reason, a greater applied moment is required to crack the member.

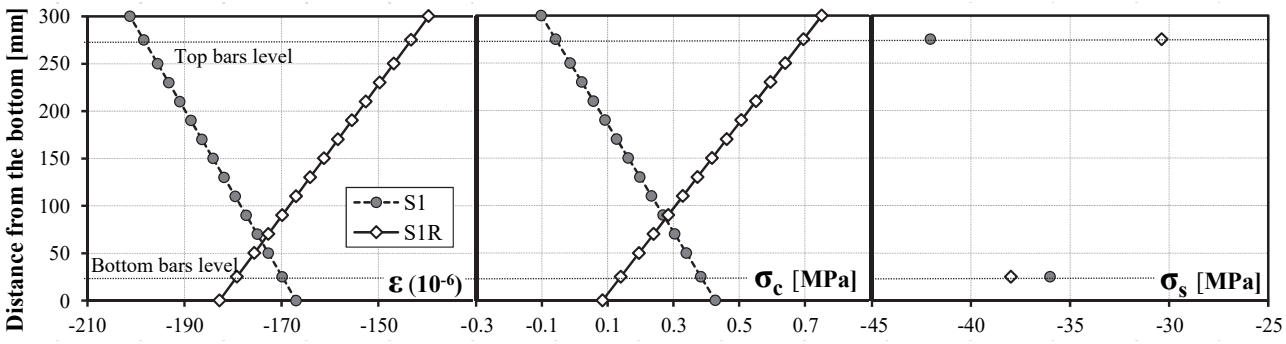

Figure 2: Numerical values of total strains ε, concrete σ_c and steel σ_s stresses within the depth of the section at midspan just before loading for beams S1 and S1R.

Numerical vs. experimental results on RC beams subjected or not to shrinkage before loading [14]

Two RC beams tested by Sato et al. [14] – named V-01-13WB and V-01-13DB – and subjected to four-point bending are selected for further comparisons. The considered specimens were characterized by the same geometry, with a rectangular cross-section (200 mm deep and 150 mm wide) and a total length equal to 2800 mm, with a net span of 2200 mm. The two beams were also characterized by the same amount of tensile reinforcement, consisting of two D13 bars. The specimens belonged to the same concrete batch, but were subjected to different curing conditions. After demolding, beam V-01-13WB was indeed sealed at room temperature with saturated paper ("Wet curing") until the time of testing, whereas beam V-01-13DB was first subjected to wet curing for one week and subsequently exposed to room atmosphere for 114 days ("Drying condition").

Sample	Steel			Concrete				
	$A_{s,bottom}$ [mm²]	E_s [GPa]	f_{sy} [MPa]	f_c [MPa]	$f_{ct,sp}$* [MPa]	E_c [GPa]	ε_{sh} (10^{-6})	φ_c
V-01-13WB	253.4	193.2	353	30.6	2.9	27.5	-	-
V-01-13DB	253.4	193.2	353	32.5	3.0	28.5	425	3.3

*: f_{ct} adopted in the analyses is calculated from $f_{ct,sp}$ according to UNI EN 1992-1-1 [16]

Table 2: Material properties of RC beams tested by Sato et al. [14]

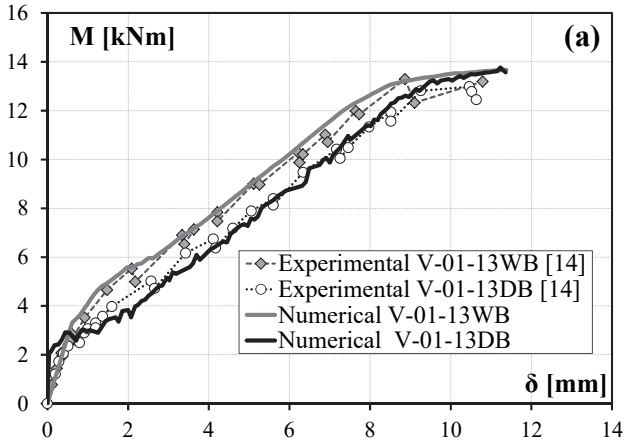

		Sample	
		V-01-13WB	V-01-13DB
$M_{cr,exp}$	[kNm]	3.6	2.1
$M_{cr,num}$	[kNm]	3.2	2.1
δ_{exp}**	[mm]	3.7	4.6
δ_{num}**	[mm]	3.7	4.7
$w_{max,exp}$**	[mm]	0.12	0.12
$w_{max,num}$**	[mm]	0.10	0.15
$w_{av,exp}$**	[mm]	0.07	0.08
$w_{av,num}$**	[mm]	0.05	0.06

**: Values at M=7.2 kNm

Figure 3: Comparison between numerical and experimental [14] results (a) in terms of bending moment M vs. midspan deflection δ; (b) under serviceability conditions, for beams V-01-13WB and V-01-13DB.

The main mechanical properties of steel and concrete, together with the average free shrinkage strain ε_{sh} and the creep coefficient φ_c at the date of testing, are summarized in Tab. 2.
Numerical analyses are performed by following the same modeling choices already described in the previous Section. Fig. 3a shows a comparison between numerical and experimental [14] results in terms of bending moment M vs. midspan deflection δ; for both the considered beams. Since initial deflection due to shrinkage was not experimentally measured, also in this case numerical curves are shifted to the origin.

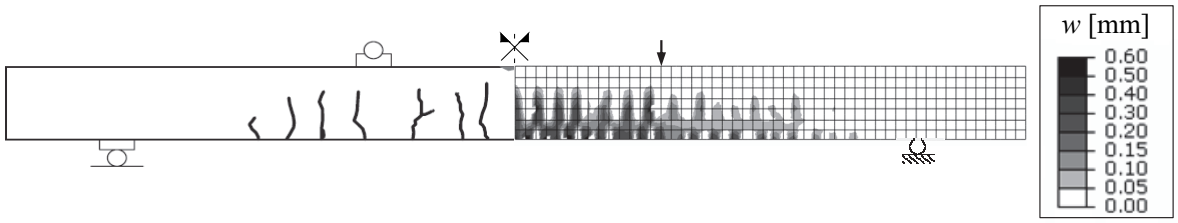

Figure 4: Numerical and experimental [14] crack pattern at failure for specimen V-01-13DB.

As can be seen from Fig. 3a, the shrunk specimen V-01-13DB is characterized by a reduced cracking load and a larger deflection with respect to sample V-01-13WB. Additional comparisons are provided in Fig. 3b, where numerical and experimental values of cracking moment M_{cr}, deflection δ, average and maximum crack width (w_{av} and w_{max}) under serviceability conditions are listed. Finally, a good agreement is also found in terms of crack pattern at failure, as proved by Fig. 4, which reports numerical and experimental results for the shrunk specimen V-01-13DB.

Conclusions

In this paper, a non-linear constitutive model for the analysis of RC structures, named 2D-PARC, is modified so as to include early-age shrinkage effects. The procedure is verified through comparisons with experimental data on RC beams subjected to short-term loadings available in the literature. Satisfactory results are obtained in terms of both global behavior and local member response (i.e. stresses in concrete/steel, crack distribution and width), thus making the model a useful tool both in engineering and research practice.

References

[1] Gilbert, R.I., Shrinkage, cracking and deflection – the serviceability of concrete structures, EJSE International, 1 (2001) 2-14.
[2] Gribniak, V., Kaklauskas, G., Kliukas, R., Jakubovskis R., Shrinkage effect on short-term deformation behavior of reinforced concrete – when it should not be neglected, Mater Design, 51 (2013) 1060-70. doi:10.1016/j.matdes.2013.05.028
[3] Bischoff, P.H., Effects of shrinkage on tension stiffening and cracking in reinforced concrete, Can J Civil Eng, 28 (2001) 363–74. doi: 10.1139/l00-117
[4] Scanlon, A., Bischoff, P.H., Shrinkage restraint and loading history effects on deflections of flexural members, ACI Struct J, 105 (2008) 498–506.
[5] Rots, J. G., De Borst R., Analysis of mixed-mode fracture in concrete, J Struct Mech, 113 (1987) 1739-1758. doi:10.1061/(ASCE)0733-9399
[6] Vecchio, F.J., Reinforced concrete membrane element formulations, ASCE J Struct Eng, 116 (1990) 730-50. doi:10.1061/(ASCE)0733-9445
[7] Maekawa, K., Soltani, M., Ishida, T., Itoyama, Y., Time-dependent space-averaged constitutive modeling of cracked reinforced concrete subjected to shrinkage and sustained loads, J Adv Concr Technol, 4 (2006) 193-207. doi:10.3151/jact.4.193
[8] Kaklauskas, G., Gribniak, V., Bacinskas, D., Vainiunas, P., Shrinkage influence on tension stiffening in concrete members, Eng Struct, 31 (2009) 1305-12. doi:10.1016/j.engstruct.2008.10.007

[9] Luo, Y., Wang, M.Y., Zhou, M., Deng, Z., Topology optimization of reinforced concrete structures considering control of shrinkage and strength failure, Comput Struct, 157 (2015) 31-41. doi:10.1016/j.compstruc.2015.05.009
[10] Cerioni, R., Iori, I., Michelini, E., Bernardi, P., Multi-directional modeling of crack pattern in 2D R/C members, Eng Fract Mech, 75 (2008) 615–28. doi:10.1016/j.engfracmech.2007.04.012.
[11] Bernardi, P., Cerioni, R., Michelini, E., Analysis of post-cracking stage in SFRC elements through a non-linear numerical approach, Eng Fract Mech, 108 (2013) 238-250. doi:10.1016/j.engfracmech.2013.02.024
[12] Bernardi, P., Cerioni, R., Michelini, E., Sirico, A., Numerical modeling of the cracking behavior of RC and SFRC shear-critical beams, Eng Fract Mech (2016) doi:10.1016/j.engfracmech.2016.04.008
[13] Gribniak, V., Shrinkage influence on tension-stiffening of concrete structures, PhD Thesis, Vilniaus Gedimino technikos universitetas, Vilnius, Lituania (2009)
[14] Sato, R., Maruyama, I., Sogabe, T., Sogo, M., Flexural behavior of reinforced recycled concrete beams, J Adv Concr Technol, 5 (2007) 43-61. doi:10.3151/jact.5.43
[15] ACI Committee 209. Guide for Modeling and Calculating Shrinkage and Creep in Hardened Concrete, ACI 209.2R-08, Farmington Hills, Michigan, (2008)
[16] UNI EN 1992-1-1:2005. Eurocode 2 – Design of concrete structures – Part 1-1: General rules and rules for buildings, (2005).
[17] Bazant, Z., P., Baweja S., Creep and shrinkage prediction model for analysis and design of concrete structures: Model B3. ACI Special Publications 194 (2000).